GRAPHENE NANOCOMPOSITES: A STUDY ON THE FAILURE BEHAVIOR AND SCALING

Yao Qiao[1], Cory Hage Mefford[1] and Marco Salviato*[1]

[1] Department of Aeronautics and Astronautics, University of Washington
Guggenheim Hall, Seattle, WA, 98195
* Corresponding Author. Email: salviato@aa.washington.edu

Keywords: Graphene, Fracture, Size effect, Damage

ABSTRACT

This work proposes an investigation on the scaling of the structural strength of polymer/graphene nanocomposites. To this end, fracture tests on geometrically scaled Single Edge Notch Bending (SENB) specimens with varying contents of graphene were conducted to study the effects of nanomodification on the scaling. It is shown that, while the strength of the pristine polymer scales according to Linear Elastic Fracture Mechanics (LEFM), this is not the case for nanocomposites, even for very low graphene contents. In fact, small specimens exhibited a more pronounced ductility with limited scaling and a significant deviation from LEFM whereas larger specimens behaved in a more brittle way, with scaling of nominal strength closer to the one predicted by LEFM.

A study on a large bulk of literature data confirmed that this is not a salient feature of polymer/graphene nanocomposites only but also of several other nanocomposites. It is shown that most of the specimen sizes investigated in the literature belong to the transitional region between ductile and brittle behavior where LEFM cannot characterize the fracturing behavior.

1 INTRODUCTION

Thanks to their outstanding specific mechanical and functional properties, the engineering use of polymer/graphene nanocomposites is becoming broader and broader. Current applications include electronics, additive manufacturing, energy storage devices and the use as nanoreinforcement for advanced carbon fiber composites [1]. However, the design of large nanocomposite structures requires capturing the scaling of their mechanical properties, an aspect often overlooked in the literature on nanocomposites. Due to the complex mesostructure characterizing graphene nanocomposites, the size of the non-linear Fracture Process Zone (FPZ) occurring in the presence of a large stress-free crack is usually not negligible [2-5]. The stress field along the FPZ is nonuniform and decreases with crack opening, due to discontinuous cracking, nano-crack deflection by graphene platelets, and frictional pullout of graphene layers [6]. Consequently, the fracturing behavior and, most importantly, the energetic size effect associated with the given structural geometry, cannot be described by means of the classical LEFM. To capture the effects of a finite, non-negligible FPZ, the introduction of a characteristic (finite) length scale related to the fracture energy and the strength of the material is necessary [2-5].

2 MATERIALS AND METHODS

2.1 Materials and preparation

The thermoset polymer used for all of the tested specimens was composed by an EPIKOTE resin and an EPIKOTE curing agent MGSTM RIMH 134 - RIMH 137 combined in a 100:36 ratio (by weight). Thanks to the low viscosity of the resin, a solvent was not used even after the addition of graphene. The nanofiller was A-12 Graphene Nanoplatelet with an average flake thickness of less than 3 nm (between 3-8 graphene monolayers) and lateral dimensions of approximately 2-8 microns. For the preparation of the epoxy/graphene specimens, the desired amount of epoxy and graphene was mixed for 10 minutes and then high shear mixed at 1500 rpm for 20 minutes by means of an electrically activated high shear mixer with a 48 mm impeller. Shear mixing was followed by

sonication using a Hielscher UP200S sonicator with a 7 mm sonotrode for 20 minutes at 70% amplitude and a duty cycle of 0.5. This latter step was required to promote a satisfactory platelet exfoliation and it had been adopted successfully by the authors for the dispersion of nanoclays in thermoset polymers [7-9].

In order to remove any air bubbles, the mixture was then degassed for 20 minutes. After degassing and adding the hardener, the mixture was manually mixed for 10 minutes and then poured into the silicone molds. It was allowed to cure at room temperature for approximately 48 hours and then post-cured in an oven for 4 hours at 60 ^{o}C.

After curing, the specimens were pre-cracked through by tapping. Tapping was preferred to sawing to create the last portion of the crack in order to provide a very sharp tip and to limit the emergence of plastic residual stresses [10]. All the crack lengths within 0.35-0.55 of the width of the specimens. More details about the materials and preparation can be found in [11].

2.2 Specimen preparation

2.2.1 Uniaxial testing

The dogbone specimens used for the uniaxial tests followed ASTM D638-02a [12]. Four material configurations, characterized by different graphene weight contents, were prepared for uniaxial tensile tests, namely: pure epoxy, 0.3 wt%, 0.9 wt%, and 1.6 wt%. The surfaces of dogbone specimens were painted white and then speckled with black paint to allow for Digital Image Correlation (DIC) analysis.

2.2.2 Fracture testing

The design of the Single Edge Notch Bending (SENB) specimens was based on ASTM D5045-99 [13]. Four sets of SENB specimens were prepared for the three-point bending tests: pure epoxy, 0.3 wt%, 0.9 wt%, and 1.6 wt% graphene nanocomposites. In order to study the scaling of the fracturing behavior, as illustrated in Fig. 1, geometrically scaled specimens of three different sizes were prepared. The dimensions, scaled as 1:2:4, were 10x36 mm, 20x72 mm, and 40x144 mm, respectively. The thickness was kept equal to 12 mm for all the sizes. The various crack lengths of the specimens were approximately in the range $0.35D$ to $0.55D$, where D is the width of the specimen.

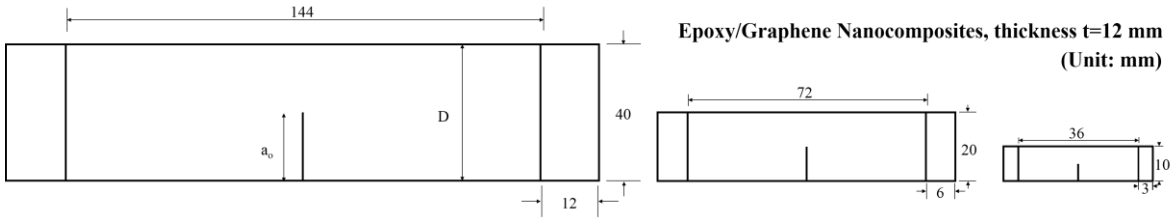

Figure 1: Geometry of Single Edge Notch Bending (SENB) Specimens. Units: mm.

2.3 Testing

The uniaxial tensile tests and three-point bending tests were performed on a closed-loop electro-activated 5585H Instron machine. The speckled dogbone specimens were analyzed by means of a Digital Image Correlation (DIC) system by Correlated Solutions [14]. The load rate for uniaxial tensile tests was 5 mm/min whereas, to avoid viscoelastic effects, the load rate for three-point bending tests was adjusted for the different sizes to achieve roughly the same average strain rate of 0.2%/min. It is worth mentioning here again that the geometrical scaling involved also the length of the initial crack which was always about 0.35-0.55 the width, D, of the specimens. The scaling did not involve the thickness, t, which was kept about 12 mm for all the investigated sizes.

2.4 Microscopic analysis

Scanning Electron Microscopy (SEM) was performed to investigate the toughening mechanisms of the material system at the nanoscale. The fracture surfaces were observed by means of a JSM-

6010PLUS/LA Electron Microscope [15] by applying an acceleration voltage of 1 kV without sputtering.

3 EXPERIMENTAL RESULTS

3.1 Fracture tests

The load-displacement curves of three-point bending tests are plotted in Fig. 2 for different graphene concentrations. It is worth noting that, for the pure epoxy specimens, the mechanical behavior is linear up to the peak load which is followed by unstable crack propagation. This is an indication of pronounced brittle behavior for all the sizes investigated. With the addition of graphene, differences in the behavior of small specimens with respect to large specimens become visible, this effect being more pronounced for higher graphene contents. In fact, while large specimens show a very linear response up to failure, a significant non-linear segment before the peak load characterizes the smaller sizes. This latter aspect indicates hardening inelastic behavior and reduced brittleness (or higher ductility) for the smallest specimen sizes. After reaching the peak load, the specimens exhibited snap-back instability for all the investigated sizes and graphene concentrations. Consequently, the failures were catastrophic (dynamic) and occurred shortly after the peak load.

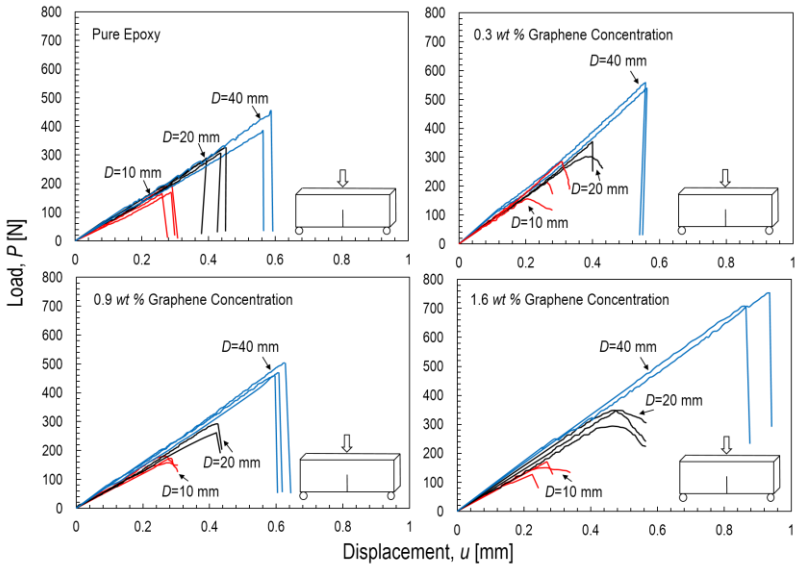

Figure 2: Load-displacement curves for different graphene concentrations and specimen sizes.

3.2 SEM analysis

In order to investigate the main nanoscale mechanisms of damage that can lead to an increase in mode I fracture energy of graphene nanocomposites, the SENB specimens were analyzed by SEM using a JSM-6010PLUS/LA Electron Microscope [15].

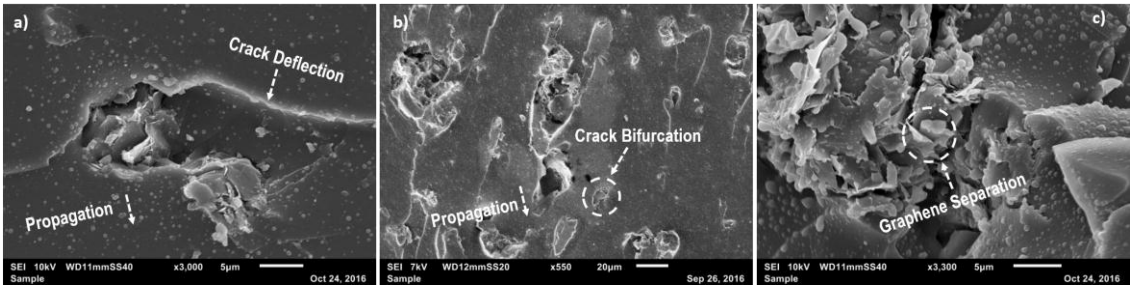

Figure 3: Damage mechanisms of graphene nanocomposites: a) crack deflection (1.6 wt% graphene concentration); b) crack pinning/bifurcation (0.9 wt% graphene concentration); c) separation between graphene layers (1.6 wt% graphene concentration).

High magnification images in the propagation region are shown in Figs. 3a-c for 0.9 wt% and 1.6 wt% graphene concentrations. Based on the pictures, the damage mechanisms are shown to be the following: a) microcrack deflection; b) microcrack pinning/bifurcation; and c) separation between graphene layers.

These damage mechanisms cause the crack to take a more torturous path thus requiring more energy to be released during the crack propagation. Similar damage mechanisms were reported in [6-9,16] for graphene nanocomposites and other nanofillers of similar morphology.

4 ANALYSIS AND DISCUSSION

4.1 Analysis of fracture tests by Size Effect Law (SEL)

The size of the non-linear FPZ occurring in the presence of a large stress-free crack is generally not negligible. Consequently, the fracturing behavior and, most importantly, the energetic size effect associated with the given structural geometry, cannot be described by means of classical LEFM. To capture the effects of a finite, nonnegligible FPZ, the introduction of a characteristic (finite) length scale related to the fracture energy and the strength of the material is necessary [2-5]. This is done in the following sections.

4.1.1 Size effect law for graphene nanocomposites

The fracture tests can be analyzed leveraging on an equivalent linear elastic fracture mechanics approach to account for the presence of a FPZ of finite size. To this end, an effective crack length $a = a_0 + c_f$ with $a_0 =$ initial crack length and $c_f =$ effective FPZ length is considered. Following LEFM, the energy release rate can be written as follows:

$$G(\alpha) = \frac{\sigma_N^2 D}{E^*} g(\alpha) \tag{1}$$

where $\alpha = a/D =$ normalized effective crack length, $\sigma_N = 3PL/2tD^2 =$ nominal stress, $E^* = E$ for plane stress and $E^* = E/(1-\nu^2)$ for plane strain, and $g(\alpha) =$ dimensionless energy release rate. The failure condition can now be written as:

$$G(\alpha_0 + c_f/D) = \frac{\sigma_{Nc}^2 D}{E^*} g(\alpha_0 + c_f/D) = G_f \tag{2}$$

where G_f is the mode I fracture energy of the material and c_f is the effective FPZ length, both assumed to be material properties. It should be remarked that this equation characterizes the peak load conditions if $g'(\alpha) > 0$, i.e. only if the structure has positive geometry [2].

By approximating $g(\alpha)$ with its Taylor series expansion at a_0 and retaining only up to the linear term of the expansion, one obtains:

$$G_f = \frac{\sigma_{Nc}^2 D}{E^*} [g(a_0) + \frac{c_f}{D} g'(\alpha_0)] \tag{3}$$

which can be rearranged as follows [2]:

$$\sigma_{Nc} = \sqrt{\frac{E^* G_f}{D g(\alpha_0) + c_f g'(\alpha_0)}} \tag{4}$$

where $g'(\alpha_0) = dg(\alpha_0)/d\alpha$.

This equation relates the nominal strength of radially scaled structures to a characteristic size, D and it can be rewritten in the following form:

$$\sigma_{Nc} = \frac{\sigma_0}{\sqrt{1 + D/D_0}} \tag{5}$$

where $\sigma_0 = \sqrt{E^* G_f / c_f g'(\alpha_0)}$ and $D_0 = c_f g'(\alpha_0)/g(\alpha_0) =$ constant, depending on both FPZ size and specimen geometry. Contrary to classical LEFM, Eq. (5) is endowed with a characteristic length scale D_0. This is key to describe the transition from ductile to brittle behavior with increasing structure size reported in the fracture tests.

4.1.2 Fitting of experimental data by SEL

The values of G_f and c_f can be determined by regression analysis of the experimental data rearranging Eq. (3) as follows:

$$\frac{1}{g'(\alpha_0)\sigma_{Nc}^2} = \frac{g(\alpha_0)}{g'(\alpha_0)E^* G_f} D + \frac{c_f}{E^* G_f} \tag{6}$$

$$Y = BX + M \tag{7}$$

where $X = g(\alpha_0)D/g'(\alpha_0)$, $Y = [g'(\alpha_0)\sigma_{Nc}^2]^{-1}$, $B = (E^* G_f)^{-1}$, and $M = c_f / E^* G_f$. Following Eq. (7), a linear regression analysis was conducted for all the graphene concentrations.

4.2 Estimation of fracture properties by SEL

The parameters of the size effect law, B and M, can be directly related to the mode I fracture energy of the material, G_f and the effective FPZ size, c_f as follows:

$$G_f = \frac{1}{E^* B},\ c_f = \frac{M}{B} \tag{8}$$

provided that the functions $g(\alpha)$, $g'(\alpha) = dg(\alpha)/\alpha$ and the elastic modulus E^* are known. The mode I fracture energy G_f and the effective FPZ length c_f estimated by means of Eqs. (8a,b) are tabulated in Table 1 whereas the calculation of $g(\alpha)$ and $g'(\alpha)$ is discussed in the next section.

Graphene concentration (wt%)	Fracture energy G_f (N/mm)	c_f (mm)
0	0.880	0.283
0.3	0.911	0.546
0.9	1.059	1.096
1.6	1.693	1.587

Table 1: Mode I fracture energy G_f and the effective Fracture FPZ c_f for different graphene concentrations.

It is worth noting here that, indeed, the addition of graphene led to an enhancement of the mode I fracture energy which increased from 0.880 N/mm for the pure epoxy case to 1.693 N/mm for the 1.6 wt% case, a 92.4% improvement. On the other hand, the addition of graphene caused a larger FPZ size which changed from 283 μm to 1587 μm. This latter aspect is of utmost importance: while the inherent assumption of LEFM of a negligible FPZ seems reasonable for the pure epoxy case, this is not true for graphene-modified specimens which show a FPZ about one order of magnitude larger and not negligible compared to e.g. the specimen width.

The importance of the finiteness of the FPZ for the estimation of nanocomposite fracture energy and its consequences on the structural scaling will be the subject of section 4.5.

4.3 Calculation of $g(\alpha)$ and $g'(\alpha)$

The function $g(\alpha)$ was obtained through Finite Element Analyses (FEA) in ABAQUS Implicit 6.13 [17]. 8-node biquadratic plain strain quadrilateral elements (CPS8) were adopted while the quarter element technique [18] was used at the crack tip to provide accurate results. The smallest element size at the tip was about $a_0.10^{-5}$ leading to roughly 11,000 elements for the whole model. A

linear elastic isotropic constitutive model was used for the simulations, with $E = 3000$ MPa and $\nu = 0.35$. The J-integral approach [19] was used to estimate the energy release rate in the presence of a concentrated load centered on the top of the SENB specimen. The final interpolated values are:

$$g(\alpha) = 1155.4\alpha^5 - 1896.7\alpha^4 + 1238.2\alpha^3 - 383.04\alpha^2 + 58.55\alpha - 3.0796 \tag{9}$$

$$g'(\alpha) = 18909\alpha^5 - 31733\alpha^4 + 20788\alpha^3 - 6461.5\alpha^2 + 955.06\alpha - 50.88 \tag{10}$$

4.4 Size effect analysis

To investigate the scaling behavior of structural strength, it is interesting to analyze perfectly radially scaled specimens of different sizes. Now that the fracture properties of the various material systems are known, it is possible to estimate the structural strength for a given normalized crack length starting from the experimental data. In fact, let us consider a crack length of $0.5\,D$ for all the specimen sizes. One can relate the experimental results, calculated for crack lengths close to $0.5\,D$ but not exactly $0.5\,D$, to the desired case by imposing that the energy release rate at failure is G_f in both cases. This leads to the following expression for the adjusted nominal strength:

$$\sigma_{Nc,desired} = \sigma_{Nc,\exp}\sqrt{\frac{Dg(\alpha_{0,\exp}) + c_f g'(\alpha_{0,\exp})}{Dg(0.5) + c_f g'(0.5)}} \tag{11}$$

The experimental data adjusted according to Eq. (11) and the fitting by SEL are shown in Figs. 4a-d where the structural strength σ_{Nc} is plotted as a function of the structure size D in double logarithmic scale. In such a graph, the structural scaling predicted by LEFM is represented by a line of slope -1/2 whereas the case of no scaling, as predicted by stress-based failure criteria, is represented by a horizontal line. The intersection between the LEFM asymptote, typical of brittle behavior, and the plastic asymptote, typical of ductile behavior, corresponds to $D = D_0$, called the *transitional size* [2].

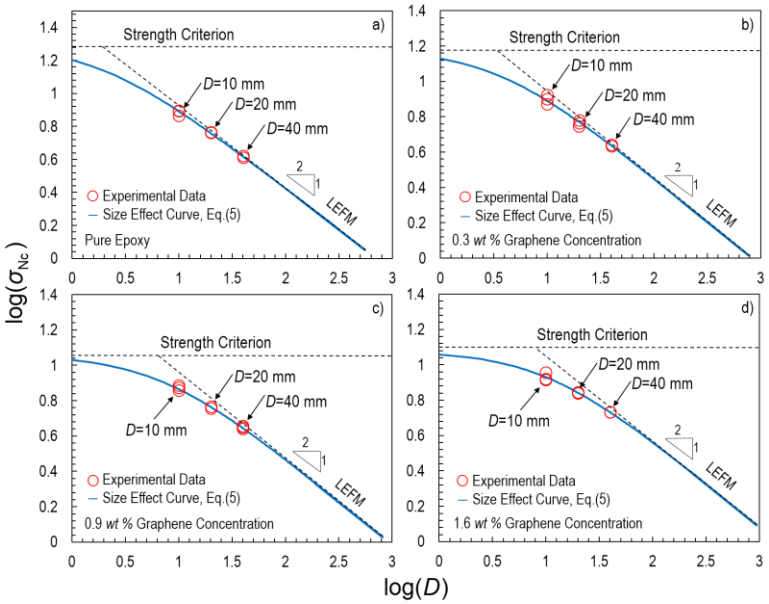

Figure 4: Size effect curves for different graphene concentrations.

As can be noted from Fig. 4a, the experimental data related to the pure epoxy system all lie very close to the LEFM asymptote showing that, for the range of sizes investigated in this work (or larger sizes), linear elastic fracture mechanics provides a very accurate description of fracture scaling. This confirms that, for the pure epoxy and sufficiently large specimens, the FPZ size has a negligible effect and LEFM can be applied, as suggested by ASTM D5045-99 [13]. However, this is not the case for graphene nanocomposites which, as Figs. 4b-d show, are characterized by a significant deviation from

LEFM, the deviation being more pronounced for smaller sizes and higher graphene concentrations. Particularly, the figures show a transition of the experimental data from stress-driven failure, characterized by the horizontal asymptote, to energy driven fracture characterized by -1/2 asymptote. This phenomenon can be ascribed to the increased size of the FPZ compared to the structure size which makes the non-linear effects caused by micro-damage in front of the crack tip not negligible. For sufficiently small specimens, the FPZ affects the structural behavior and causes a significant deviation from the scaling predicted by LEFM with a much milder effect of the size on the structural strength. On the other hand, for increasing sizes, the effects of the FPZ become less and less significant thus leading to a stronger size effect closely captured by LEFM. Further, comparing the size effect plots of nanocomposites with different graphene concentrations, it can be noted a gradual shift towards the ductile region thus showing that not only the addition of graphene leads to a higher fracture toughness but also to a gradually more ductile structural behavior for a given size.

The foregoing conclusions are extremely important for the design of graphene nanocomposite structures or electronic components. As the experimental data show, LEFM does not always provide an accurate method to extrapolate the structural strength of larger structures from lab tests on small-scale specimens, especially if the size of the specimens belonged to the transitional zone. In fact, the use of LEFM in such cases may lead to a significant underestimation of structural strength, thus hindering the full exploitation of graphene nanocomposite fracture properties. This is a severe limitation in several engineering applications such as e.g. aerospace or aeronautics for which structural performance optimization is of utmost importance. On the other hand, LEFM always overestimates significantly the strength when used to predict the structural performance at smaller length-scales. This is a serious issue for the design of e.g. graphene-based MEMS and small electronic components or nanomodified carbon fiber composites in which the inter-fiber distance occupied by the resin is only a few micrometers and it is comparable to the FPZ size. In such cases, SEL or other material models characterized by a characteristic length scale ought to be used.

4.5 LEFM vs SEL for the estimation of fracture properties of nanocomposites

Having discussed the scaling of the fracturing behavior and having shown that, for graphene nanocomposites, the FPZ is not negligible for the range of specimen sizes investigated, it is interesting to check how the mode I fracture energy calculated through SEL compares to the estimation from LEFM for the various sizes and graphene contents. The fracture energy can be calculated by means of LEFM as follows:

$$G(\alpha_0) = \frac{\sigma_N^2 D}{E^*} g(\alpha_0) \tag{12}$$

where all the quantities and functions have the same meaning discussed in previous sections but, different from SEL, the FPZ length is not accounted for. Figs. 5a-c show a comparison between the fracture energy estimated by SEL and by LEFM for different specimen sizes and graphene concentrations. As can be noted, for a given size, the difference between SEL and LEFM increases with the amount of graphene with LEFM underestimating G_f. The difference increases with the addition of graphene since, as shown in previous sections, the FPZ size increases monotonically and thus the cardinal assumption of LEFM becomes less and less accurate. The underestimation caused by LEFM can be very significant if one considers that the maximum difference, occurring at 1.6 wt% for all sizes, is 20.9%, 49.2% and even 113.3% for the large, medium and small sizes respectively. More importantly, a serious issue about using LEFM when the specimen sizes belong to the transitional region is that the estimate is not objective, i.e. it does depend on the size of the specimen tested. This can be noted from Figs. 5a-c which show that, for a given graphene content, the fracture energy estimated by LEFM is size dependent, being lower for smaller sizes. It is interesting to note that, for example, the calculations based on LEFM for 1.6 wt% nanocomposites show basically no increment in the fracture energy for the small size specimen while, for the large size, the increment is about 50%. Conversely, thanks to the characteristic length scale associated with the FPZ size, SEL provides the same estimate of the fracture energy for all the sizes. Of course, the size dependence of the fracture energy estimated by LEFM and its difference from SEL depends on the range of sizes investigated: for

sufficiently large specimens, both the theories provide the same, size independent, fracture energy. However, as will be shown in the following sections, most of the tests on nanocomposites reported in the literature were performed on small specimens belonging to the transitional region between ductile and brittle behavior. This may explain why the range of fracture energy increments obtained by nanomodification reported in the literature is so large: neglecting the effects of the non-linear FPZ lead to fracture energy estimates which were size dependent and consistently underestimating, the underestimation being more significant for larger nanofiller concentrations and smaller specimen sizes.

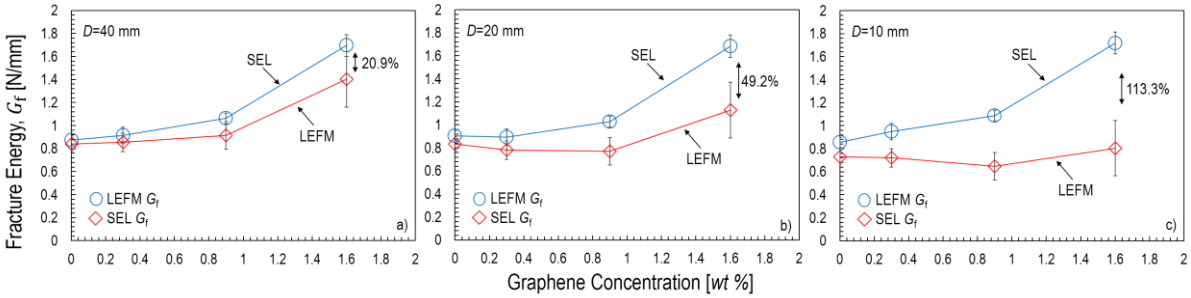

Figure 5: Fracture energy estimated from LEFM and SEL for the specimen sizes and graphene contents investigated in this work.

5 SIZE EFFECT ANALYSIS OF LITERATURE DATA

5.1 Application of SEL to general nanocomposites

To understand if the quasi-brittle behavior is a salient feature of graphene nanocomposites only or if it characterizes other nanocomposites, the foregoing analysis was extended on a large bulk of literature data. In order to study the effects of the FPZ, the data were re-analyzed by SEL. The expression for the corrected fracture energy has the following form:

$$G_{f,SEL} = G_{f,LEFM}\left[1-\frac{\beta E^* g'(\alpha_0) G_{f,LEFM}}{D f_t^2 g(\alpha_0)}\right]^{-1} \tag{13}$$

where $G_{f,LEFM} = \sigma_{Nc}^2 D g(\alpha_0)/E^*$, f_t is ultimate strength of the specimens, and c_f is replaced by $\beta E^* G_f / f_t^2$. In this analysis, in the absence of data on c_f, β is assumed to be 0.44 which, according to Cusatis *et al*. [20], corresponds to the assumption of a linear cohesive law. For the publications where SENB specimens were tested, the curves for $g(\alpha)$ and $g'(\alpha)$ discussed in section 4.3 can be used. It can be observed from Eq. (13) that the correct fracture energy in the literature can be calculated by knowing three key parameters provided that $g(\alpha)$ and $g'(\alpha)$ are known: (1) The fracture energy through the use of LEFM; (2) The Young's modulus of the specimens at different nanoparticle concentrations; and (3) The ultimate strength of the specimens at different nanoparticle concentrations. The ultimate strength, Young's modulus, and Poisson's ratio of nanocomposites were reasonably assumed to be 50 MPa, 3000 MPa, and 0.35, respectively, for cases in which those parameters were not provided by the authors.

5.2 Results for corrected fracture energy of general nanocomposites

Different types of nanofillers were investigated in this re-analysis in order to study the effects of the FPZ on nanocomposites. These nanofillers can be summarized into the following: (1) carbon-based nanofillers such as carbon black, graphene oxide, graphene nanoplatelet, and multi-wall carbon nanotube; (2) other nanofillers such as rubber, silica, and nanoclay. The fracture energies estimated from LEFM compared to the calculation through are plotted in Figs. 6-7 along with the highest percent difference for each data set was labeled.

Carolan *et al*. [21] investigated the SENB specimens nanomodified by six different combinations of nanofillers as shown in Fig. 6. The fracture energy percent difference between LEFM and SEL

varied based on the nanofiller used, with the greatest difference being 42.6% for the addition of 8 wt% core shell rubber mixed with 25% diluent and 8% silica.

As can be seen from Fig. 7, the SENB specimens nanomodified by three different sizes of silica nanoparticles were reported by Zamanian *et al*. [22]. The greatest percent difference of fracture energy between LEFM and SEL decreased as the size of silica nanoparticle increased, with the greatest difference being 28% for the addition of 6 wt% 12 nm silica nanoparticles whereas the lowest difference being 19.5% for the addition of 7.5 wt% 40 nm silica nanoparticles. On the other hand, Jiang *et al*. [23] investigated relatively large SENB specimens, compared to the other specimens in the literature re-analyzed, nanomodified by three different types of nanofillers. As can be noted, the greatest percent increase in fracture energy between LEFM and SEL reached up to 51.8% for silica nanoparticle attached graphene oxide thus the size of specimen is not sufficiently large to guarantee the use of LEFM to characterize the fracturing behavior.

Kim *et al*. [24] investigated the SENB specimens nanomodified by nanoclay and carbon black respectively (Fig. 7). In this case, the specimen size was enough to justify the use of LEFM as confirmed by the low difference with SEL (11.2% for nanoclay and 7.3% for carbon black). Similar conclusions can be drawn on the silica nanoparticles investigated by Vaziri *et al*. [25]. However, for the three different sizes of silica nanoparticles investigated by Dittanet *et al*. [26], a significant difference between LEFM and SEL was observed in silica nanoparticles, confirming that all the specimens tested belonged to the transition zone between ductile and brittle behavior.

As Fig. 7 shows, a comparison between SENB specimens nanomodified by Polyethersulfone (PES) functionalized and nonfunctionalized multi-wall carbon nanotube reported by Konnola *et al*. [27] shows a higher difference with values ranging from 15.5% to 20.3% in fracture energy. On the other hand, Liu *et al*. [28] investigated the CT specimens nanomodified by four different combinations of silica nanoparticle and rubber. As the plots show, neglecting the significant effects of FPZ leads to a tremendous deviation between LEFM and SEL, the fracture energy being underestimated up to about 157% and this effect being more significant for larger nanofiller contents.

The analysis showed that most of the specimen sizes considered in the literature belong to the transitional region, i.e. they exhibit a quasi-brittle behavior. Consequently, the non-negligible FPZ size plays a pivotal role in obtaining size independent fracture energy which cannot be characterized through the use of LEFM. Comparing the literature data with a SEL re-analysis showed that the fracture energy is generally underestimated with differences that sometimes are higher than 150% depending on the size of the specimens tested and the amount of nanofiller. In general, these differences increase with the amount of nanofiller since the size of the FPZ generally increases with the nanofiller content.

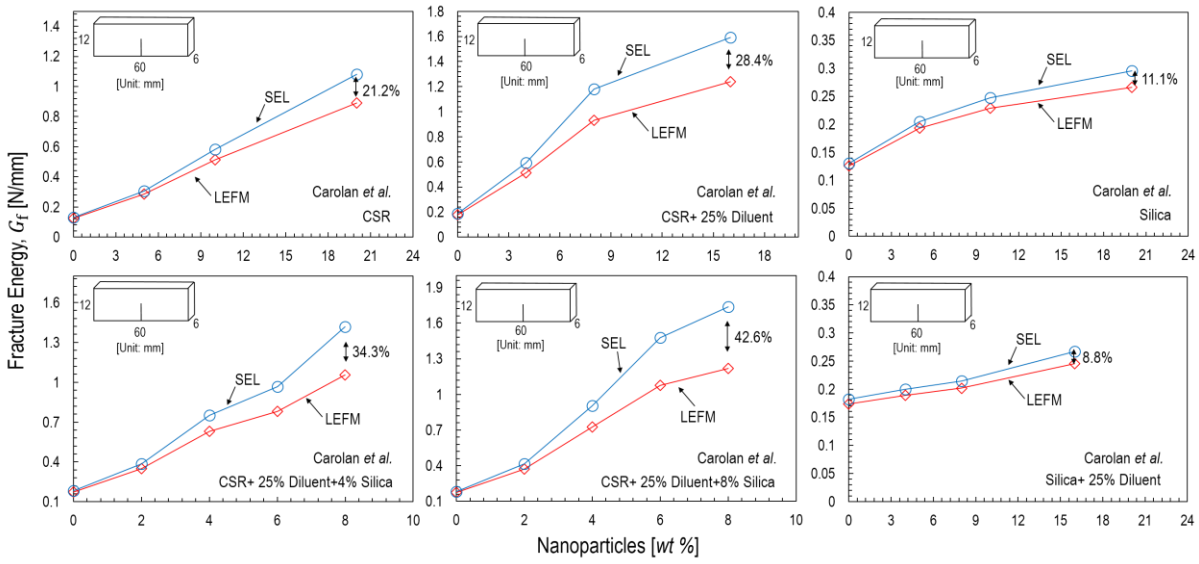

Figure 6: Comparative Analysis of LEFM G_f and SEL G_f values from [21].

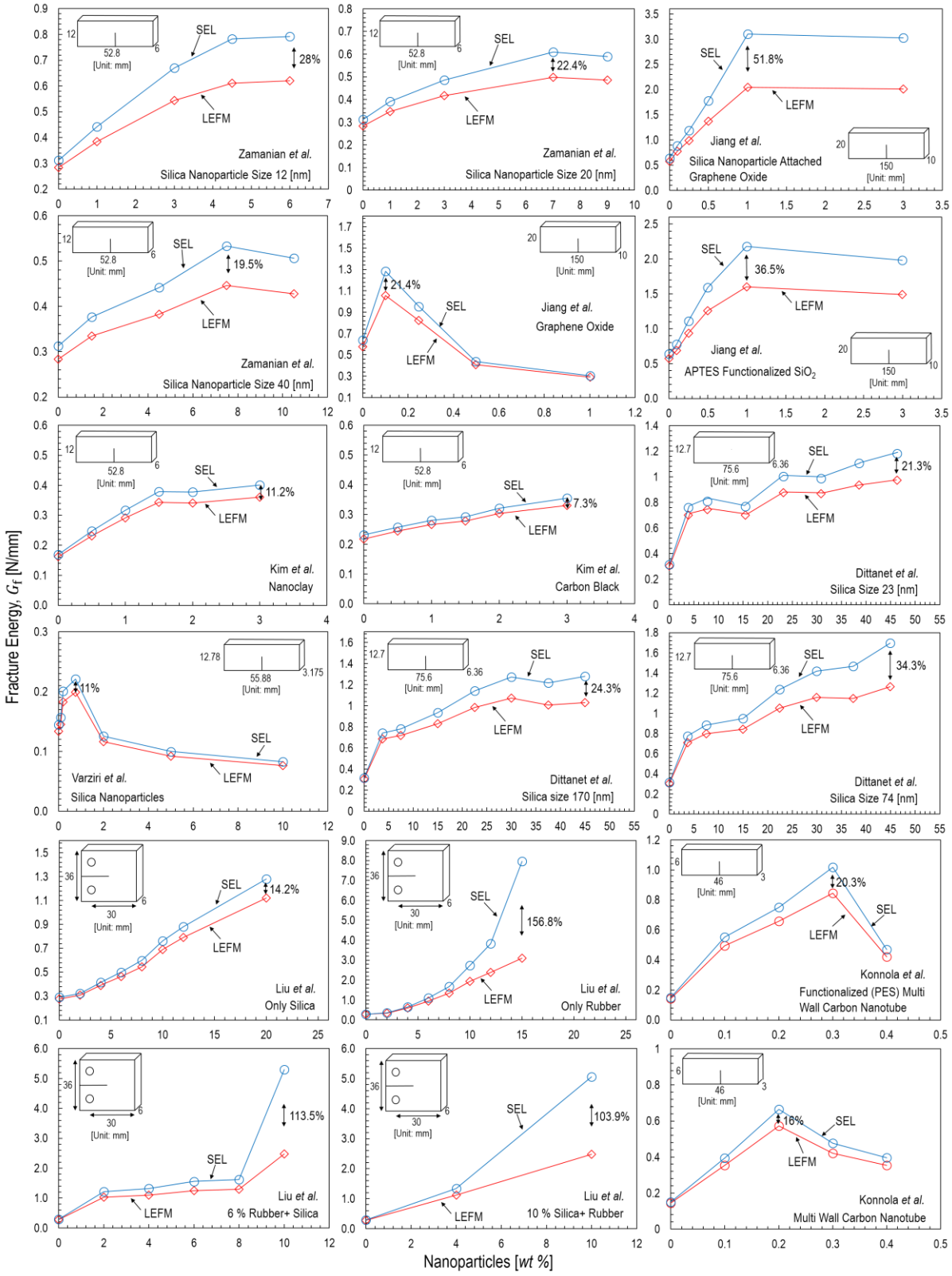

Figure 7: Comparative Analysis of LEFM G_f and SEL G_f values from [21-28].

6 CONCLUSIONS

1. For all the investigated contents, the addition of graphene nanoplatelets to the resin did not provide a significant effect on the elastic properties and strength whereas an outstanding enhancement of mode I fracture energy was reported. A weight fraction of 1.6% of graphene resulted in an increase

of the fracture energy of about 92.4% compared to the pristine resin, this result making graphene-modified resins ideal candidates for the development of tougher composite structures;

2. The fracture tests on geometrically scaled SENB specimens confirmed a remarkable size effect. The analysis of the experimental data showed that the fracture scaling of the pure epoxy is captured accurately by Linear Elastic Fracture Mechanics (LEFM). However, this was not the case for graphene nanocomposites which exhibited a more complicated scaling. The double logarithmic plots of the nominal stress as a function of the characteristic size of the specimens showed that the fracturing behavior evolves from ductile to brittle with increasing sizes. For sufficiently large specimens, the data tend to the classical -1/2 asymptote predicted by LEFM. However, for smaller sizes, a significant deviation from LEFM was reported, a behavior associated to a more pronounced ductility. This trend was more and more pronounced for increasing graphene contents;

3. The deviation from LEFM reported in the experiments is related to the size of the Fracture Process Zone (FPZ) for increasing contents of graphene. In the pure epoxy the damage/fracture zone close to the crack tip, characterized by significant non-linearity due to subcritical damaging, was generally very small compared to the specimen sizes investigated. This was in agreement with the inherent assumption of LEFM of negligible non-linear effects during the fracturing process. However, the addition of graphene nanoplatelets resulted in larger and larger FPZs. For sufficiently small specimens, the size of the highly nonlinear FPZ was not negligible compared to the specimen characteristic size thus highly affecting the fracturing behavior, this resulting into a significant deviation from LEFM;

4. Capturing the correct scaling of the fracturing behavior is of utmost importance for structural design. Further, it is quintessential to correctly measure important material properties such as the fracture energy. The analysis of the results reported in this study shows that using LEFM to calculate the mode I fracture energy from the experiments leads to a size dependent G_f. Taking the specimens with 1.6% wt of graphene as an example, the fracture energy according to LEFM was 0.8 N/mm, 1.0 N/mm and 1.25 N/mm for the small, medium and large sizes respectively. The reason for this discrepancy is that LEFM lacks intrinsically of a characteristic length and thus cannot capture the effects of the FPZ size;

5. Following Bažant [2,4,5], an Equivalent Fracture Mechanics approach was used to introduce a characteristic length, c_f, into the formulation. This length is related to the FPZ size and it is considered a material property as well as G_f. An excellent agreement with experimental data is shown, with SEL capturing the transition from quasi-ductile to brittle behavior with increasing sizes. The fracture energy for the specimens with 1.6% wt of graphene, finally a material property independent of the specimen size, was 1.69 N/mm whereas c_f =1.59 mm;

6. The difference between the fracture energy predicted by LEFM and SEL depends on the FPZ size compared to the specimen size, with LEFM underestimating G_f compared to SEL. For the specimens with 1.6% wt of graphene and the sizes considered in this work, LEFM predictions were about 113.3%, 49.2% and 20.9% lower compared to SEL for the small, medium and large sizes respectively. The difference decreases with increasing specimen sizes and tends to zero for sufficiently large specimens as the FPZ becomes negligible compared to the specimen size;

7. The foregoing analysis was then extended to a large bulk of literature data on nanocomposites showing that size effect is a salient feature of these materials. The analysis showed that most of the specimen sizes considered in the literature belong to the transitional region, i.e. they exhibit a quasi-brittle behavior. Notwithstanding this, the totality of the fracture energies calculated in the literature relies on the use of LEFM and thus is not size objective. Comparing the literature data with a SEL reanalysis showed that the fracture energy is generally underestimated with differences that sometimes are higher than 150% depending on the size of the specimens tested and the amount of nanofiller. In general, these differences increase with the amount of nanofiller since the size of the FPZ generally increases with the nanofiller content;

8. The foregoing evidences show that particular care should be devoted to the understanding of the scaling of the fracture behavior of nanocomposites. Particularly, the fracture tests carried out to characterize e.g. the fracture energy should guarantee objective results. Size effect testing on geometrically scaled specimens is a simple and effective approach to provide objective data. Alternatively, LEFM could be used provided that the specimen size is large enough. The size limit

depends on the size of the FPZ and is generally higher than the one suggested by ASTM D5045-99.

REFERENCES

[1] Rogers JA. Electronic materials: making graphene for microelectronics. Nat Nanotechnol 2008;**3**:254-55.

[2] Bažant ZP, Planas J. Fracture and size effect in concrete and other quasi-brittle materials. Boca Raton:CRC Press;1998.

[3] Salviato M, Kirane K, Ashari SE, Bažant ZP. Experimental and numerical investigation of intra-laminar energy dissipation and size effect in two-dimensional textile composites. Compos Sci Technol 2016;**135**:67-75.

[4] Bažant ZP. Size effect in blunt fracture: concrete, rock, metal. J Eng Mech-ASCE 1984;**110**(4):518-35.

[5] Bažant ZP, Kazemi MT. Determination of fracture energy, process zone length and brittleness number from size effect, with application to rock and concrete. Int J Fracture 1990;**44**:111-31.

[6] Chandrasekaran S, Sato N, Tölle F, Mülhaupt R, Fiedler B, Schulte K. Fracture toughness and failure mechanism of graphene based epoxy composites. Compos Sci Technol 2014;**97**:90-99.

[7] Quaresimin M, Salviato M, Zappalorto M. Fracture and interlaminar properties of clay-modified epoxies and their glass reinforced laminates. Eng Fract Mech 2012;**81**:80-93.

[8] Zappalorto M, Salviato M, Quaresimin M. Mixed mode (I+II) fracture toughness of polymer nanoclay nanocomposites. Eng Fract Mech 2013;**111**:50-64.

[9] Zappalorto M, Salviato M, Pontefisso A, Quaresimin M. Notch effect in clay-modified epoxy: a new perspective on nanocomposite properties. Compos Interfaces 2013;**20**(6):405-19.

[10] Xiao K, Ye L, Kwok YS. Effects of precracking methods on fracture behaviour of an Araldite-F epoxy and its rubber-modified systems. J Mater Sci 1998;**33**(11):2831-36.

[11] Mefford CH, Yao Q, Salviato M. Failure and Scaling of Graphene Nanocomposites, arXiv:1702.05828, 2017.

[12] ASTM D638-02a - Standard Test Method for Tensile Properties of Plastics 2003.

[13] ASTM D5045-99 - Standard Test Methods for Plane-Strain Fracture Toughness and Stain Energy Release Rate of Plastic Materials 1999.

[14] Correlated Solutions, Columbia, USA http://www.correlatedsolutions.com.

[15] Jeol, Tokyo, Japan http://www.jeol.co.jp/en/.

[16] Chandrasekaran S., Seidel C., Schulte K. Preparation and characterization of graphite nano-platelet (GNP)/epoxy nano-composite: mechanical, electrical and thermal properties. Eur Polym J 2013;**49**(12):3878-88.

[17] ABAQUS, v., ABAQUS User's Manual, Version 6.13-1, Hibbit, Pawtucket, RI. 2013.

[18] Barsoum R. A degenerate solid element for linear fracture analysis of plate bending and general shells. Int J Numer Meth Eng 1976;**10**(3):551-64.

[19] Rice J. A path independent integral and the approximate analysis of strain concentration by notches and cracks. J Appl Mech 1968;**35**(2):379-86.

[20] Cusatis G, Schauffert EA, Cohesive crack analysis of size effect, Eng Fract Mech 2009;**76**(14), 2163-73.

[21] Carolan D, Ivankovic A, Kinloch AJ, Sprenger S, Taylor AC. Toughening of epoxy-based hybrid nanocomposites. Polymer 2016;**97**:179-190.

[22] Zamanian M, Mortezaei M, Salehnia B, Jam JE. Fracture toughness of epoxy polymer modified with nanosilica particles: particle size effect. Eng Fract Mech 2013;**97**:193-206.

[23] Jiang T, Kuila T, Kim NH, Ku BC, Lee JH. Enhanced mechanical properties of silanized silica nanoparticle attached graphene oxide/epoxy composites. Compos Sci Technol 2013;**79**:115-25.

[24] Kim BC, Park SW, Lee DG. Fracture toughness of the nano-particle reinforced epoxy composite. Compos Struct 2008;**86**(1-3):69-77.

[25] Vaziri HS, Abadyan M, Nouri M, Omaraei IA, Sadredini Z, Ebrahimnia M. Investigation of the fracture mechanism and mechanical properties of polystyrene/silica nanocomposite in various silica contents. J Mater Sci 2011;**46**(17):5628-38.

[26] Dittanet P, Pearson R. Effect of silica nanoparticle size on toughening mechanisms of filled epoxy Polymer 2012;**53**:1890-1905.

[27] Konnola R, Nair CPR, Joseph K. High strength toughened epoxy nanocomposite based on poly(ethersulfone)-grafted multi-walled carbon nanotube. Polym Advan Technol 2015;**27**(1):82-89.

[28] Liu HY, Wang GT, Mai YW, Zeng Y. On fracture toughness of nano-particle modified epoxy. Compos Part B-Eng 2011;**42**(8):2170-75.